

Inclusion of Carrier-Carrier-Scattering Into Arbitrary-Order Spherical Harmonics Expansions of the Boltzmann Transport Equation

K. Rupp^{*†}, P.W. Lagger^{*}, T. Grasser^{*}, and A. Jünger[†]

^{*}Institute for Microelectronics, TU Wien, Gußhausstraße 27–29/E360, A-1040 Wien, Austria

[†]Institute for Analysis and Scientific Computing, TU Wien, Wiedner Hauptstraße 8–10/E101, A-1040 Wien, Austria
E-mail: rupp@iue.tuwien.ac.at

Abstract—A methodology for handling carrier-carrier-scattering within the arbitrary-order spherical harmonics expansion method for computing deterministic numerical solutions of the Boltzmann transport equation is presented. Comparisons with results from Monte Carlo simulations confirm the accuracy of the proposed method for bulk silicon. Moreover, results for 22nm and 110nm MOSFET devices are presented. A significant elevation of the high-energy-tail of the distribution function is observed in the 22nm case, confirming that the inclusion of carrier-carrier-scattering is required for the investigation of hot-carrier-effects in scaled-down devices.

I. INTRODUCTION

The deterministic Spherical Harmonics Expansion (SHE) method for the numerical solution of the Boltzmann Transport Equation (BTE) has become an attractive alternative to the stochastic Monte-Carlo (MC) method thanks to significantly shorter execution times [1], [2]. While the method has long been essentially limited to one-dimensional device simulations due to memory constraints, modern workstations provide enough resources for running two- and even three-dimensional simulations [3], [4]. Also, excellent agreement with MC results became only possible after the method had been extended to arbitrary expansion orders [5].

Despite the availability of a suitable formalism for a wide range of common scattering operators such as phonon scattering and ionized impurity scattering, the inclusion of carrier-carrier scattering (cc-scattering) has so far only been considered in a very early publication for first-order SHE in bulk silicon [6]. A suitable formalism for the consideration of cc-scattering with higher-order expansions, a broader range of dispersion relations [7], or device simulation has not been available so far. In this work we present a methodology for the inclusion of carrier-carrier scattering into arbitrary-order SHE and discuss the implications on the computational effort as well as the memory requirements.

II. CARRIER-CARRIER SCATTERING FOR SHE

Using a low-density approximation and thus neglecting the Pauli-principle, most scattering mechanisms lead to a linear scattering operator. In contrast, cc-scattering leads to a quadratic scattering operator of the form

$$Q_{cc}\{f\} = \int_{\mathcal{B}^3} s(\mathbf{k}', \mathbf{k}, \mathbf{k}'_2, \mathbf{k}_2) f(\mathbf{k}') f(\mathbf{k}'_2) - s(\mathbf{k}, \mathbf{k}', \mathbf{k}_2, \mathbf{k}'_2) f(\mathbf{k}) f(\mathbf{k}_2) d(\mathbf{k}', \mathbf{k}_2, \mathbf{k}'_2), \quad (1)$$

where f is the carrier distribution function, \mathcal{B} denotes the Brillouin zone, \mathbf{k} , \mathbf{k}_2 , \mathbf{k}' , \mathbf{k}'_2 are linked with momentum \mathbf{p} via the semiclassical relation $\mathbf{p} = \hbar\mathbf{k}$ and for simplicity termed *wave vectors* in the following, cf. Fig. 1, and $s = \sigma_{cc} \delta(\varepsilon + \varepsilon_2 - \varepsilon' - \varepsilon'_2) \delta(\mathbf{k} - \mathbf{k}' + \mathbf{k}_2 - \mathbf{k}'_2)$ equipped with delta distributions ensures conservation of energy and momentum, respectively. Here and in the following all dependencies on the spatial variable \mathbf{x} and time t are suppressed for the sake of clarity. The coefficient σ_{cc} is proportional to

$$\sigma_{cc}(\mathbf{k}, \mathbf{k}', \mathbf{k}_2, \mathbf{k}'_2) \simeq \frac{n}{[(\mathbf{k} - \mathbf{k}')^2 + 1/\lambda_D^2]^2}, \quad (2)$$

includes the local carrier density n , the Debye-length λ_D , and shows a strong angular dependence, cf. Fig. 2. Note that the denominator of σ_{cc} depends on the initial and the final state of one of the two particles only, thus $\sigma_{cc}(\mathbf{k}, \mathbf{k}', \mathbf{k}_2, \mathbf{k}'_2) = \sigma_{cc}(\mathbf{k}, \mathbf{k}')$. Moreover, since the denominator is identical to that from ionized impurity scattering, we treat it in the same way using an isotropic approximation with identical momentum relaxation times [8], [9].

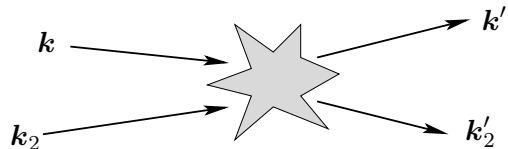
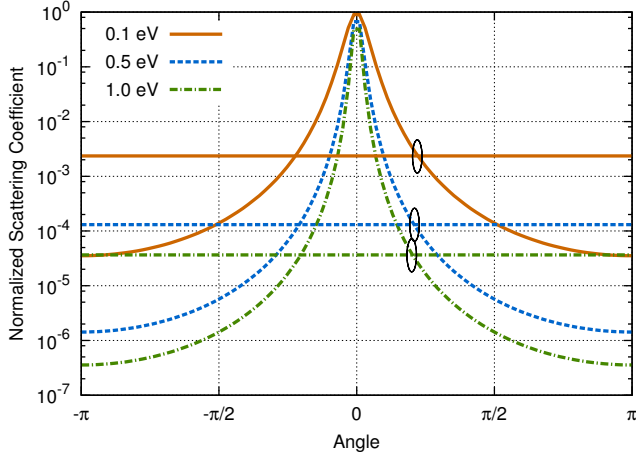
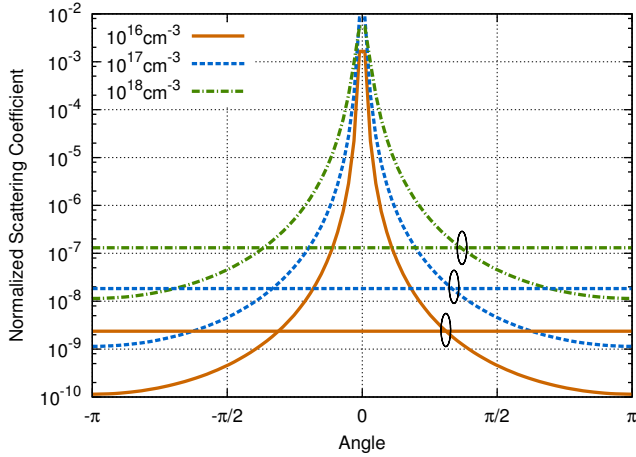


Fig. 1. Wavevectors \mathbf{k} and \mathbf{k}_2 of two carriers prior to scattering with each other, and wavevectors \mathbf{k}' and \mathbf{k}'_2 after scattering. Momentum and energy are conserved.



(a) Constant carrier density $n = 10^{18} \text{ cm}^{-3}$.



(b) Constant energy 0.5 eV.

Fig. 2. Comparison of the anisotropic carrier-carrier scattering coefficient and the isotropic approximation with respect to the angle $\theta = \angle(\mathbf{k}, \mathbf{k}')$ for different carrier concentrations and carrier energies (normalized). The anisotropy is particularly pronounced at high energies and small carrier concentrations.

In a first step momentum conservation is used to eliminate integration over the wave vector \mathbf{k}_2 of the second incident particle in (1), leading to

$$Q_{cc}\{f\} = \int_{\mathcal{B}^2} \left[\sigma_{cc}(\mathbf{k}', \mathbf{k}) f(\mathbf{k}') f(\mathbf{k}_2) - \sigma_{cc}(\mathbf{k}, \mathbf{k}') f(\mathbf{k}) f(\mathbf{k}' + \mathbf{k}_2 - \mathbf{k}) \right] \times \delta(\varepsilon + \varepsilon^* - \varepsilon' - \varepsilon'_2) d(\mathbf{k}', \mathbf{k}'_2) \quad (3)$$

with $\varepsilon^* = \varepsilon(\mathbf{k}' + \mathbf{k}'_2 - \mathbf{k})$. In general, the energy ε^* of the second particle involved in the scattering process cannot be written in a closed-form representation, or an explicit dispersion relation may not be available at all [7]. Consequently, we assume for the moment that ε^* is a known (but not necessarily constant) value.

Splitting the scattering operator into in-scattering and out-scattering, $Q_{cc}\{f\} = Q_{cc;\text{in}}\{f\} - Q_{cc;\text{out}}\{f\}$, rewriting (3) using spherical coordinates $(\varepsilon, \theta, \varphi)$ in momentum space, and expanding the distribution function into spherical harmonics via

$$f(\mathbf{k}) = \sum_{l,m} f_{l,m}(\varepsilon) Y_{l,m}(\theta, \varphi) \quad (4)$$

leads after elimination of ε'_2 , the use of the modified isotropic scattering rate $\sigma_{cc;\text{iso}}$ and an isotropic density of states Z to

$$Q_{cc;\text{in}}\{f\} = \sum_{l',m',l_2,m_2'} \int_0^\infty \int_0^\infty \sigma_{cc;\text{iso}}(\varepsilon', \varepsilon) \times \int_{\Omega} \int_{\Omega} Y_{l',m'} Y_{l_2,m_2'} d\Omega' d\Omega'_2 \times f_{l_2,m_2'}(\varepsilon + \varepsilon^* - \varepsilon') Z(\varepsilon + \varepsilon^* - \varepsilon') \times f_{l',m'}(\varepsilon') Z(\varepsilon') d\varepsilon' d\varepsilon'_2 \quad (5)$$

for the in-scattering operator, and to

$$Q_{cc;\text{out}}\{f\} = \sum_{l,m,l_2,m_2} \int_0^\infty \int_0^\infty \sigma_{cc;\text{iso}}(\varepsilon, \varepsilon') \times \int_{\Omega} \int_{\Omega} Y_{l,m} Y_{l_2,m_2}(\theta^*, \varphi^*) d\Omega d\Omega_2 \times f_{l,m}(\varepsilon) Z(\varepsilon) f_{l_2,m_2}(\varepsilon^*) Z(\varepsilon^*) d\varepsilon d\varepsilon_2 \quad (6)$$

for the out-scattering operator. With the additional assumption that $f(\varepsilon^*) = f_{0,0}(\varepsilon^*) Y_{0,0}$, i.e. the distribution of the second particle is given by an isotropic distribution, all integrals over the unit sphere can be computed analytically using the orthonormality of spherical harmonics.

The SHE method in addition requires the cc-scattering operator Q_{cc} to be projected onto each of the spherical harmonics $Y_{l,m}$. A multiplication with $Y_{l,m}$ and a delta distribution for the integration over spheres of constant energy [5] ultimately yields with an integration over the whole momentum space

$$Q_{cc;l,m}\{f\} = \frac{Z}{Y_{0,0}^3} \int_0^\infty \sigma_{cc} [f_{0,0}(\varepsilon') f_{0,0}(\varepsilon + \varepsilon^* - \varepsilon') - f_{0,0}(\varepsilon^*) f_{l,m}(\varepsilon)] \times Z(\varepsilon') Z(\varepsilon + \varepsilon^* - \varepsilon') d\varepsilon' \quad (7)$$

Note that the scattering operator vanishes for the case of f being given by a Maxwell distribution and is thus consistent with other scattering mechanisms.

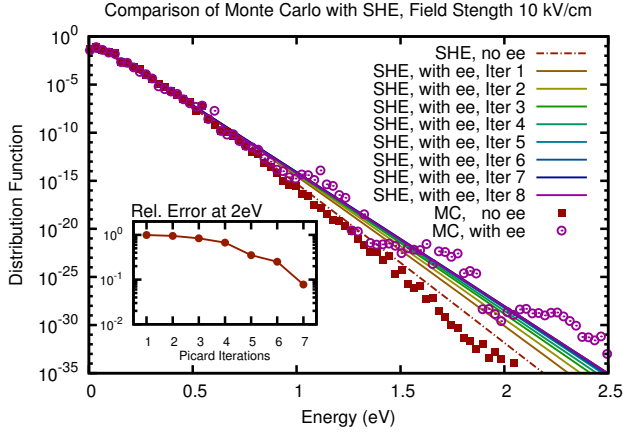


Fig. 3. Simulation of the electron distribution with and without electron-electron scattering in bulk silicon at an applied field of 10 kV/cm. The elevation of the distribution function at higher energies as obtained by the MC method is well reflected by SHE with our proposed methodology. After at most eight nonlinear Picard iterations, the change of the distribution function becomes negligible (see inset).

Since the energy ε^* of the second particle is unknown by nature, we propose a weighted average over all energies with respect to the distribution function in the current iterate. As a computationally cheaper alternative, one may also set ε^* to the average carrier energy at the respective location inside the device at the price of possibly reduced accuracy.

III. RESULTS

The proposed model is implemented in our free open-source simulator ViennaSHE [10]. A single valley in the conduction band using the non-parabolic Modena dispersion relation is considered. The energy ε^* of the second incoming particle is set to the average carrier energy at the respective location in the device for all simulations.

Simulation results for bulk silicon are compared with MC-results in Fig. 3 and Fig. 4. It can clearly be seen that our method is able to resolve the high energy tails of the distribution function well. Only a few additional nonlinear Picard iterations are sufficient for convergence. It is interesting to observe that less iterations are required for an electric field of 100 kV/cm as compared to 10 kV/cm, even though the corrections to the distribution function due to cc-scattering are larger.

In Fig. 5 our method is applied to self-consistent simulations of two MOSFET devices with different channel lengths. An elevation of the high-energy tail due to cc-scattering is particularly observed for the

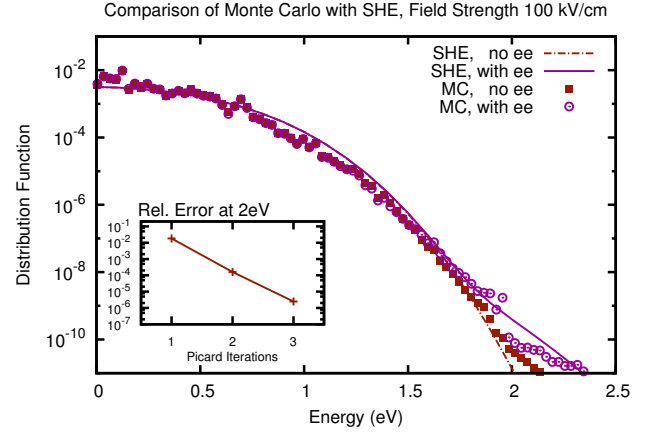


Fig. 4. Simulation of the electron distribution with and without electron-electron-scattering in bulk silicon at an applied field of 100 kV/cm. The high-energy tail of the distribution function around 2 eV is essentially resolved by the proposed method after only one nonlinear Picard iteration.

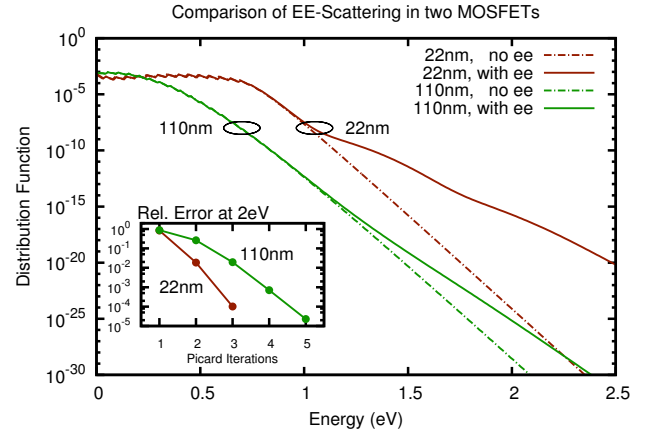


Fig. 5. Comparison of the electron energy distribution function at channel-drain transition region for a 22nm and a 110nm MOSFET device with $V_{DS} = 1.0$ Volt and $V_G = 0.8$ Volt. The influence of cc-scattering on the high-energy tail of the distribution function is particularly pronounced in the smaller device. After at most three Picard iterations, convergence for practical purposes is obtained. The ripples at lower energies are due to optical phonon scattering.

smaller device, emphasizing the importance of cc-scattering for predictive device simulation. Again, the nonlinear iteration converges faster for the smaller device despite the larger impact on the shape of the distribution function for higher energies.

The implications of the proposed scheme on hardware requirements are evaluated in Fig. 6. While the number of unknowns of the linear system obtained in each nonlinear iteration step remains unchanged, the convolution-type integral expression for $Q_{cc;l,m}$ in (7) couples all energies for each node x in the device

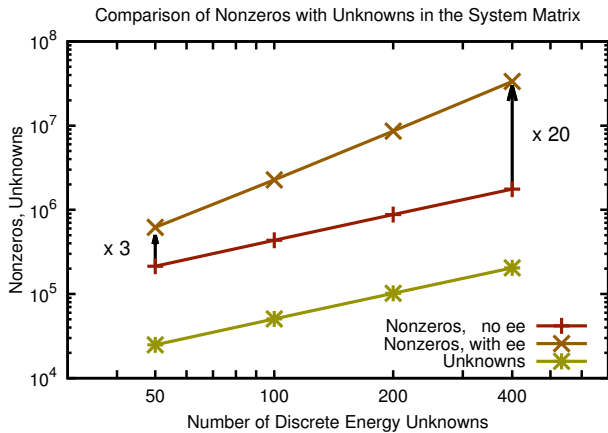


Fig. 6. Nonzeros and number of unknowns of the system matrix for a 22nm MOSFET device. While both the number of unknowns and the number of nonzeros in the system matrix scale linearly with the number of energy points, carrier-carrier scattering leads to a coupling of all energy points, leading to quadratic effort. Memory requirements are consequently increased by a factor of three using 50 discrete energy unknowns per node in the spatial mesh and up to a factor of 20 when using 400 points in total energy direction. With typically 100 to 200 energy points per electron Volt, one thus has to expect increased memory requirements of one order of magnitude for an applied bias between one and two Volt.

mesh with each other, which leads to a quadratic dependence of the computational effort on the number of discrete energy unknowns per node in the spatial mesh. It has to be noted that the rise in the overall memory consumption and simulation time is smaller than suggested by the increase in the number of unknowns. This is due to the observation that lower preconditioner fill-in [5] is encountered, or the use of block-diagonal preconditioners [4] which ignore couplings between different energies.

IV. CONCLUSION

We have suggested a formulation that allows for the inclusion of cc-scattering into arbitrary-order SHE. Even though the description of carrier-carrier scattering by means of (1) and (2) is widely accepted, further interactions such as dynamic carrier screening [11] are not accounted for in this setting. Nevertheless, an initial comparison shows good agreement with bulk MC results. Moreover, our method can also be used in one-, two- or three-dimensional device simulations. Due to much shorter simulation times and the absence of stochastic noise, our method is very attractive for detailed studies of hot-carrier effects.

ACKNOWLEDGMENTS

The authors wish to thank P. Palestri and A. Zaka for providing Monte Carlo data for comparison. K. Rupp and A. Jüngel gratefully acknowledge support by the Graduate School PDETech at the TU Wien. K. Rupp, T. Grasser and A. Jüngel acknowledge support by the Austrian Science Fund (FWF), grant P23598.

REFERENCES

- [1] N. Goldsman, L. Henrickson, and J. Frey, A Physics-Based Analytical/Numerical Solution to the Boltzmann Transport Equation for the Use in Device Simulation. *S.-S. Electr.*, vol. 34, p. 389–396, 1991.
- [2] A. Gnudi, D. Ventura, and G. Baccarani, One-Dimensional Simulation of a Bipolar Transistor by means of Spherical Harmonics Expansion of the Boltzmann Transport Equation. *Proc. SISDEP*, vol. 4, p. 205–213, 1991.
- [3] S.-M. Hong, A.-T. Pham, C. Jungemann, *Deterministic Solvers for the Boltzmann Transport Equation*. Springer, 2011.
- [4] K. Rupp, T. Grasser, and A. Jüngel, On the Feasibility of Spherical Harmonics Expansions of the Boltzmann Transport Equation for Three-Dimensional Device Geometries. *IEDM Techn. Digest*, 2011.
- [5] C. Jungemann, A.-T. Pham, B. Meinerzhagen, C. Ringhofer, M. Bollhöfer, Stable Discretization of the Boltzmann Equation based on Spherical Harmonics, Box Integration, and a Maximum Entropy Dissipation Principle. *J. Appl. Phys.*, vol. 100, no. 2, p. 024502+, 2006.
- [6] A. Ventura, A. Gnudi, and G. Baccarani, Inclusion of Electron-Electron Scattering in the Spherical Harmonics Expansion Treatment of the Boltzmann Transport Equation. *Proc. SISDEP*, vol. 5, p. 161-164, 1993.
- [7] S. Jin, S.-M. Hong, C. Jungemann, An Efficient Approach to Include Full-Band Effects in Deterministic Boltzmann Equation Solver Based on High-Order Spherical Harmonics Expansion. *IEEE Trans. El. Dev.*, vol. 58, no. 5, p. 1287–1294, 2011.
- [8] C. Jungemann and B. Meinerzhagen. *Hierarchical Device Simulation*. Springer, 2003.
- [9] M. Lundstrom. *Fundamentals of Carrier Transport*. Cambridge University Press, 2000.
- [10] ViennaSHE. <http://viennashe.sourceforge.net/>
- [11] P. Lugli and D. Ferry, Effect of Electron-Electron and Electron-Plasmon Interactions on Hot Carrier Transport in Semiconductors. *Phys. B+C*, vol. 129, p. 532-536, 1985.